9810 *Biochemistry* **2009,** *48,* 9810–9822
DOI: 10.1021/bi9014192

BIOCHEMISTRY
including biophysical chemistry & molecular biology
Article

Structure and Inhibition of Human Diamine Oxidase[†,‡]

Aaron P. McGrath,[§] Kimberly M. Hilmer,[∥] Charles A. Collyer,[§] Eric M. Shepard,[∥] Bradley O. Elmore,[∥] Doreen E. Brown,[∥] David M. Dooley,*[,⊥] and J. Mitchell Guss*[,§]

[§]*School of Molecular and Microbial Biosciences, University of Sydney, Sydney, NSW 2006, Australia,* [∥]*Department of Chemistry and Biochemistry, Montana State University, Bozeman, Montana 59717, and* [⊥]*Office of the President, University of Rhode Island, Kingston, Rhode Island 02881*

Received August 13, 2009; Revised Manuscript Received September 17, 2009

ABSTRACT: Humans have three functioning genes that encode copper-containing amine oxidases. The product of the AOC1 gene is a so-called diamine oxidase (hDAO), named for its substrate preference for diamines, particularly histamine. hDAO has been cloned and expressed in insect cells and the structure of the native enzyme determined by X-ray crystallography to a resolution of 1.8 Å. The homodimeric structure has the archetypal amine oxidase fold. Two active sites, one in each subunit, are characterized by the presence of a copper ion and a topaquinone residue formed by the post-translational modification of a tyrosine. Although hDAO shares 37.9% sequence identity with another human copper amine oxidase, semicarbazide sensitive amine oxidase or vascular adhesion protein-1, its substrate binding pocket and entry channel are distinctly different in accord with the different substrate specificities. The structures of two inhibitor complexes of hDAO, berenil and pentamidine, have been refined to resolutions of 2.1 and 2.2 Å, respectively. They bind noncovalently in the active-site channel. The inhibitor binding suggests that an aspartic acid residue, conserved in all diamine oxidases but absent from other amine oxidases, is responsible for the diamine specificity by interacting with the second amino group of preferred diamine substrates.

Copper-containing amine oxidases (CAOs)[1] are widespread throughout nature. They catalyze the oxidative deamination of primary amines to the corresponding aldehydes with the concomitant production of hydrogen peroxide and ammonia:

$$RCH_2NH_2 + O_2 + H_2O \rightarrow RCHO + H_2O_2 + NH_3$$

Whereas the primary function of the bacterial and yeast proteins is believed to be the provision of essential carbon and nitrogen compounds for metabolism, amine oxidases likely have a wide variety of roles in higher organisms. One proposed role in plants is based on the proposition that the H_2O_2 product of the reaction provides a signal for wound healing. Mammals have up to four functioning genes (AOC1−4) for CAOs (*1*). AOC2 encodes a retina-specific amine oxidase (RAO) that includes a putative transmembrane domain. Likewise, AOC3 encodes membrane-bound protein, termed vascular adhesion protein-1 or VAP-1, and AOC4 encodes a homologous soluble form of VAP-1 lacking the transmembrane domain. AOC1 encodes a diamine oxidase (DAO).

In humans, the AOC4 gene contains a mutation at position 225 which introduces a stop codon that translates to a nonfunctional truncated protein (*1*). Of the remaining three human CAOs, VAP-1 and RAO have 65% identical sequences, whereas DAO is only ~38% identical to either VAP-1 or RAO. Previously thought to be expressed specifically in retinal ganglion cells (*2*, *3*), AOC2 mRNA has recently been shown to be present in many tissues, however with RAO enzymatic activity isolated to the eye (*4*).

Interest in VAP-1 intensified when it was discovered that this endothelial glycoprotein is involved in leucocyte extravasation at sites of inflammation and that its enzymatic activity was required for the cell adhesion function (*5*−*9*). Humans have a soluble protein that has been suggested to be a proteolytic cleavage product of membrane-bound VAP-1 (*10*) functioning in place of the nonfunctional AOC4 gene product. VAP-1 has been shown to be upregulated at sites of inflammation (*10*) and has been implicated in such human diseases as diabetes mellitus (*11*, *12*), congestive heart failure (*13*), and liver disease (*10*).

DAO was originally identified as the enzyme that cleared exogenous histamine from minced lung and liver samples and was therefore termed histaminase (*14*). Subsequently, a protein identified as diamine oxidase was termed amiloride-binding protein and was incorrectly implicated with the amiloride-sensitive Na^+ channel (*15*). Consequently, some databases still designate AOC1 as ABP1. The fact that DAO and ABP1 were in fact the same protein was later noted by the original authors (*16*), who also reported the cloning of the human gene, corresponding to a 751-residue protein (*17*). Overexpression of recombinant human DAO (hDAO) has been achieved in insect cells (*18*).

[†]This research was supported by grants from the Australian Research Council (LP0669658 to C.A.C. and J.M.G.) and from the National Institutes of Health (GM 27659 to D.M.D.). A.P.M. was supported by an Australian Postgraduate Award for Industry.

[‡]The atomic coordinates and associated structure factors have been deposited in the Protein Data Bank (PDB) as entries 3HI7, 3HIG, and 3HII.

*To whom correspondence should be addressed. D.M.D.: telephone, (401) 874-4462; fax, (401) 874-7149; e-mail, davedooley@uri.edu. J.M.G.: telephone, +61-2-9351-4302; fax, +61-2-9351-5858; e-mail, m.guss@usyd.edu.au.

[1]Abbreviations: 2HP, 2-hydrazinopyridine; ABTS, 2,2′-azinobis-(3-ethyl)benzthiozoline-6-sulfonic acid; AGAO, *Arthrobacter globiformis* amine oxidase; BRN, berenil; BSAO, bovine serum amine oxidase; CAO, copper-containing amine oxidase; hDAO, human diamine oxidase; ECAO, *Escherichia coli* amine oxidase; HPAO, *Hansenula polymorpha* amine oxidase; HRP, horseradish peroxidase; MOBA, 4-(4-methylphenoxy)-2-butyn-1-amine; NOBA, 4-(2-naphthyloxy)-2-butyn-1-amine; PPLO, *Pichia pastoris* amine oxidase; PNT, pentamidine; PSAO, pea seedling amine oxidase; RAO, retina-specific amine oxidase; rmsd, root-mean-square deviation; TPQ, trihydroxyphenylalanine quinone; VAP-1, vascular adhesion protein-1.

 Published on Web 09/18/2009

The availability of large amounts of recombinant hDAO enabled the identification of its preferred substrates in vitro showing, not surprisingly, a distinct preference for diamines. In particular, two atypical diamines, histamine and 1-methyl histamine, are excellent substrates. Each contains an imidazole group in place of one of the primary amines present in typical substrates. hDAO is the frontline enzyme for degradation of exogenous histamine (*19*), and reduced levels of DAO have been shown to be directly correlated with histamine intolerance (reviewed in ref *20*). In particular, an uncomplicated pregnancy is believed to be dependent on the balance between DAO and histamine in the placenta (reviewed in ref *21*). While DAO has a broad specificity for various diamines acting on cadaverine (1,5-diaminopentane), putrescine (1,4-diaminobutane), and the polyamine spermidine, it shows low activity for the more "traditional" CAO substrates such as benzylamine and methylamine (*18*). DAO is most strongly expressed in the placenta (*18*), in the kidney (*22*, *23*), throughout the gut (*24*, *25*), and in the lung, with lower levels in the brain (*18*, *22*). A model for release of DAO by intestinal and kidney epithelial cells has been proposed (*19*, *26*) whereby DAO is liberated from basolateral vesicles at the plasma membrane in response to an external stimulus from heparin and is thereafter cleared rapidly from the circulation.

To date, structures of copper amine oxidases have been determined from all kingdoms of life with the notable exception of archaea. The structures from eubacteria (*Escherichia coli* and *Arthrobacter globiformis*), yeast (*Hansenula polymorpha* and *Pichia pastoris*), plants (*Pisum sativum*), and mammals (*Homo sapiens* and *Bos taurus*) are homodimers with a common architecture (*27*) with subunits of ~700 amino acid residues. The *E. coli* enzyme was the first structure to be determined and was described as a mushroom with the stalk formed from the two D1 domains and the cap from the D2, D3, and D4 domains of each subunit (*28*). The two active sites, located in the D4 domains, contain the Cu ions and the characteristic trihydroxyphenylalanine quinone (TPQ) cofactor. TPQ is formed post-translationally from a tyrosine residue in a spontaneous reaction in the presence of Cu ions and molecular oxygen. The ping-pong enzymatic reaction involves a reductive half in which the substrate amine reacts with the TPQ to form a Schiff base and an oxidative half involving the release of the aldehyde product and reoxidation of the enzyme with molecular oxygen. All the other structures resemble that from *E. coli* except that they lack the D1 or stalk domain.

The TPQ in CAO structures has been observed in two distinct conformations. In the "off-copper" or "active" conformation of the enzyme, the TPQ is seen to be swung away from the Cu ion toward the base of the active-site channel making available the O5 atom of the quinone for attack by the substrate amine. In the "on-copper" or "inactive" conformation, the O4 atom of the TPQ is seen to be coordinating the Cu ion, effectively restricting access of substrate to the TPQ. This conformation has also been previously observed to be correlated with the movement of a "gate" residue into position to further block access of the substrate to the TPQ (*29*).

The substrate channels of the CAOs from different organisms have very different dimensions, in keeping with their different substrate preferences (*30*). The *P. pastoris* enzyme that has a unique ability among the structurally characterized CAOs to oxidize peptidyl lysine residues has an exceptionally wide and open substrate channel. Another defining characteristic of the CAOs is the presence of an internal "lake" that has been proposed to provide a secondary rear route to and from the active site for small substrates and products during both the TPQ biogenesis and enzymatic reactions (*27*).

The structural determinants of substrate binding and the enzyme mechanism of CAOs have been examined by the determination of the structures of inhibitor complexes of many of the enzymes. Some of these inhibitors, such as 2-hydrazinopyridine and benzylhydrazine, act as nonhydrolyzable substrate analogues and bind covalently to the TPQ cofactor mimicking the formation of the Schiff base intermediate (*31*, *32*). Others are mechanism-based inhibitors that were designed to be attacked by the active-site base. The structures of complexes of MOBA [4-(4-methylphenoxy)-2-butyn-1-amine] and NOBA [4-(2-naphthyloxy)-2-butyn-1-amine] of *A. globiformis* amine oxidase AGAO showed surprisingly that they first acted as substrates and subsequently that the aldehyde products were attacked by the amino quinol of the reduced enzyme to form a covalent adduct (*33*). Other inhibitors, such as molecular wires originally designed to probe the transfer of an electron to the TPQ, bind noncovalently in the active-site channel of AGAO (*34*). Clonidine binds to a hydrophobic pocket in bovine serum amine oxidase (BSAO) close to the TPQ that is consequently forced into its on-Cu inactive conformation (*35*). Berenil [1,3-bis(4′-amidinophenyl)triazene (BRN)] and pentamidine [1,5-bis(4-amidinophenoxy)pentane (PNT)] are diamine derivatives that act as drugs used to treat trypanosomiasis and pneumocystis pneumonia infections by binding in the minor groove of DNA (*36*, *37*). Each of the two compounds has an amidophenyl moiety at either end, and they differ only in the length and chemical nature of the central linkers. We have shown that both compounds are excellent inhibitors of hDAO.

Here we describe the X-ray structure of hDAO at 1.8 Å resolution and its complexes with the inhibitors berenil and pentamidine. This work provides an explanation for the substrate specificity of a diamine oxidase, provides further possibilities for inhibitor design, and demonstrates that potent inhibition of (at least) diamine oxidases may be achieved by reversible (noncovalent) binding.

EXPERIMENTAL PROCEDURES

Protein Expression and Purification. Enzyme expression and purification were conducted as previously described (*18*). Briefly, recombinant hDAO was overexpressed as a secreted enzyme in *Drosophila* S2 cells under the control of a metallothionein promoter. Protein purification was conducted using heparin affinity, hydroxyapatite, and gel-filtration chromatographies. At all stages of the purification, sample fractions containing hDAO were pooled on the basis of catalytic activity. Activities were monitored using a coupled assay measuring the production of H_2O_2 in the presence of substrate (10 mM putrescine), chromogen stock solution {ABTS [2,2′-azinobis(3-ethyl)benzthiozoline-6-sulfonic acid]}, and horseradish peroxidase (HRP) (*38*). Assays were conducted at 37 °C in a final volume of 2 mL. HRP activation by H_2O_2 and subsequent oxidation of ABTS were monitored spectrophotometrically at 414 nm. Purified hDAO was subsequently dialyzed (10 kDa molecular mass cutoff, Pierce) against 3 × 500 mL changes of 50 mM HEPES (pH 7.2) and 150 mM KCl at 4 °C and concentrated to ~10 mg/mL in preparation for protein crystallization experiments.

Enzyme Kinetics. Compound screening studies were performed in 50 mM HEPES (pH 7.2) with the ionic strength

increased to 150 mM by KCl. The coupled assay as described in ref *18* was utilized in all the experiments, with freshly prepared vanillic acid, 4-aminoantipyrine, and the potential inhibitors being incorporated into the buffer before each set of experiments. Isoniazid, cimetidine, clonidine hydrochloride, pentamidine isethionate salt, and diminazene aceturate (berenil) all were purchased through Sigma-Aldrich. Assays were performed at 37 °C, and reactions were initiated by the addition of freshly prepared putrescine. None of the compounds tested was oxidized by hDAO under these conditions.

Control kinetic parameters were determined with amine substrate in the absence of inhibitor to enable comparisons to kinetic constants in the presence of inhibitor. For the control curves, substrate inhibition was apparent at higher putrescine concentrations [≈600−2000 μM levels (data not shown)]. When experimental data were fit to a substrate inhibition model, an average K_i value for putrescine substrate inhibition of 2270 ± 140 μM was obtained. This effect might be explained by amine substrate binding to both oxidized and substrate-reduced forms of the enzyme (*39*). For our purposes, data analysis in the presence of inhibitor compounds was limited to putrescine levels of ≤500 μM, where the effects of substrate inhibition are negligible.

A sample of purified hVAP-1 was kindly provided by D. J. Smith (Biotie Therapies Corp., Turku, Finland). Amine oxidase activity was determined by monitoring benzaldehyde production over the course of 5 min at 250 nm using an extinction coefficient of 12800 M^{-1} cm^{-1} (*40*). Assays were run in 100 mM potassium phosphate buffer (pH 7.2) at 37 °C.

Kinetic data in the presence of each inhibitor compound were collected for the first 45 s of the reaction, and initial rates were determined. Kinetic rates were then analyzed using the statistical software package GraphPad Prism (version 4.03, GraphPad Software, San Diego, CA) as previously described (*41*). Data were fit using global nonlinear regression analysis. Competitive, uncompetitive, noncompetitive, and mixed type ($1 < \alpha < \infty$ and $\beta = 0$) inhibition models from Segel were entered into GraphPad as user-defined models (*42*). In each case, the appropriate mode of inhibition was judged by the model that best fit the experimental data as determined by analysis of the statistical parameters built into GraphPad. During the curve fitting process, the inhibition constant was defined as a global parameter. Therefore, the K_i values reported here represent the best-fit values for the respective data sets.

Crystallization and X-ray Data Collection. Two different crystal forms of hDAO have been grown and characterized during the course of this work. The structures reported in this paper are all of the second form, but since the structure was originally determined by molecular replacement using the form 1 crystals, this work is described briefly for the sake of completeness.

Initial vapor diffusion hanging drop crystallization trials were set up using a Mosquito robot (Molecular Dimensions) to dispense drops consisting of 200 nL of protein solution and 200 nL of reservoir solution over a reservoir of 75 μL at 20 °C. Initial hits of platelike crystals were observed in 0.1 M MES (pH 6.5) and 12% (w/v) PEG 20K from the NeXtal Classics screen (Qiagen) after approximately 2 months. Fine screening with manually pipetted drops comprising 2 μL each of protein and reservoir solutions yielded the best crystals when the reservoir contained 0.1 M MES (pH 6.1) and 12% (w/v) PEG 20K. These orthorhombic crystals in space group $C222_1$ are termed form 1.

Subsequently, a new stock of hDAO was subjected to similar screening protocols. In this case, the initial PACT screen (Qiagen) with the Mosquito robot and 200 + 200 nL drops gave promising crystals in 0.1 M bis-tris propane (pH 7.5), 20% (w/v) PEG 3350, and 0.2 M sodium sulfate at 20 °C. Larger crystals were grown under the same conditions from manual 2 + 2 μL drops. These crystals grew to a suitable size (largest dimension being ∼200 μm) within 2 weeks. These form 2 crystals are also orthorhombic but in space group $P2_12_12_1$.

Synchrotron radiation diffraction data for the native and BRN structures were collected at Australian Synchrotron beamline AUS 3BM1 on an ADSC Quantum 210r CCD detector at a wavelength of 0.957 Å. In-house data for the PNT structure were recorded on a Mar345 image plate (Marresearch) using Cu Kα X-rays produced by a Rigaku RU200H rotating anode generator using Osmic optics (both from Rigaku).

Structure Solution and Refinement. In-house data collected from form 1 crystals were processed using DENZO and SCALEPACK (*43*). A search model of a monomer for molecular replacement was created using a template model [hVAP-1, PDB entry 2c10 (*44*)] and a sequence alignment of hDAO and the template protein using CHAINSAW (*45*). All water molecules and metal ions were removed from the search model, and side chains were pruned to common atoms based on the sequence alignment. Molecular replacement with PHASER (*46*) gave a clear solution (*Z* score = 29.1, and log likelihood gain = 590) for the data in space group $C222_1$ with one molecule in the asymmetric unit. The resulting model was first refined as a rigid body with REFMAC5 (*47*) followed by multiple rounds of restrained refinement with simulated annealing in PHENIX (*48*). Between rounds of refinement, the model was manually corrected using sigma-A-weighted electron density maps in COOT (*49*). Synchrotron radiation diffraction data were subsequently recorded on the same crystal to a resolution of 2.11 Å. The data were integrated with MOSFLM (*50*) and scaled together with the in-house data using SCALA (*51*). The in-house data were first reprocessed with MOSFLM for ease of data management. The combined data set was 95.2% complete with an R_{merge} of 0.11. The model refinement protocol used for the in-house structure described above was followed. It was evident throughout refinement that many sections of the model were disordered. Further, the R and R_{free} values converged to somewhat high values, 0.24 and 0.30, respectively.

Data collected from form 2 crystals (native and inhibitor−protein complexes) were processed using the HKL2000 software suite (*43*). For the native structure, a search model for molecular replacement was generated using the partially refined form 1 dimer stripped of solvent molecules, metal ions, and carbohydrate and with the TPQ cofactor modeled as alanine. A clear molecular replacement solution was obtained using PHASER (*Z* score = 57.0, and log likelihood gain = 9134). Following the same protocol as the form 1 structure, initial rigid body refinement was followed by multiple rounds of restrained positional and *B* factor refinement with REFMAC5. It was evident from the early rounds of refinement that the electron density maps revealed many of the disordered regions not able to be modeled in the form 1 structure. Following each round of refinement, the model was manually checked and corrected against the corresponding electron density maps in COOT. Water molecules were added as the refinement progressed either manually or automatically in COOT and checked for sufficient electron density, correct stereochemistry, and reasonable *B* factors compared to those of surrounding atoms. N-Linked carbohydrate was well-resolved in the electron density at six of the eight putative sites

Table 1: Diffraction Data and Refinement Statistics for hDAO

	native	berenil complex	pentamidine complex
Data Collection			
space group	$P2_12_12_1$	$P2_12_12_1$	$P2_12_12_1$
cell dimensions *a*, *b*, *c* (Å)	92.5, 94.8, 196.5	92.7, 94.9, 196.4	92.5, 94.7, 196.3
X-ray source	AUS 3BM1	AUS 3BM1	rotating anode
λ (Å)	0.95663	0.95663	1.5418
detector	ADSC Quantum 210r	ADSC Quantum 210r	MAR345
resolution range (Å)	46.6−1.8 (1.80−1.86)[a]	50−2.09 (2.09−2.18)[a]	50−2.15 (2.15−2.23)[a]
no. of observed reflections	1012186	468085	267279
no. of unique reflections	158683	98904	89751
completeness (%)	99 (95.1)[a]	96.7 (91.8)[a]	95.0 (87.1)[a]
multiplicity	6.4 (5.2)[a]	4.7 (4.4)[a]	3.0 (2.4)[a]
$\langle I/\sigma(I)\rangle$	20 (3.7)[a]	10.8 (2.4)[a]	9.9 (2.7)[a]
R_{merge}[b]	0.084 (0.436)[a]	0.139 (0.61)[a]	0.103 (0.336)[a]
Refinement Statistics			
no. of reflections in the working set	150455	93778	85093
no. of reflections in the test set	8007	5059	4554
no. of protomers per ASU	2	2	2
total no. of atoms (non-H)	12989	12772	12686
no. of protein atoms	11632	11587	11529
no. of metal atoms	6	6	6
no. of water molecules	1136	952	916
no. of atoms in alternate conformers	268	219	164
no. of other atoms	215	227	235
R_{cryst}	0.161 (0.221)	0.168 (0.210)	0.182 (0.232)
R_{free}	0.189 (0.259)	0.210 (0.267)	0.221 (0.301)
rmsd for bond lengths (Å)	0.011	0.012	0.008
rmsd for bond angles (deg)	1.4	1.4	1.2
$\langle B\rangle$ (Å^2)	17.5	21.0	26.4
Cruickshanks DPI[c]	0.107	0.199	0.246
DPI based on *R* factor	0.102	0.167	0.190
PDB entry	3HI7	3HIG	3HII

[a]Values in parentheses are for the highest-resolution shell. [b]$R_{merge} = \sum|I_h - \langle I_h\rangle|/\sum\langle I_h\rangle$. [c]Diffraction Precision Indicator as output from REFMAC5 (*53*).

Table 2: Inhibition of hDAO by Selected Pharmaceutical Compounds

inhibitor	mode of inhibition	inhibition constant (K_i)
isoniazid	noncompetitive	970 ± 50 μM
cimetidine	mixed	90 ± 14 μM
clonidine	mixed	100 ± 8 μM
pentamidine	mixed	290 ± 19 nM
berenil	mixed	13 ± 1 nM
pentamidine[a]	noncompetitive	1.10 ± 0.04 μM

[a]Results for hVAP-1.

(belonging to the Asn-X-Thr sequon, where X can be any residue) and modeled as the appropriate glycans during refinement. The largest peaks in the electron density corresponded to the active-site copper atoms and four secondary cation binding sites. The secondary sites were modeled as Ca^{2+} ions on the basis of (i) the homology of Ca^{2+} binding sites in the related copper amine oxidase structures of *P. pastoris* [PDB entry 1w76 (*30*)] and VAP-1 [PDB entry 2c10 (*44*)], (ii) their relative peak heights, and (iii) the corresponding anomalous difference electron density peaks. The TPQ was modeled into unbiased omit density during the final stages of refinement. The quality of the structures was analyzed using MOLPROBITY (*52*).

The starting model for the refinement of the structures of the protein−inhibitor complexes was the refined native structure with solvent molecules, metal ions, and carbohydrate removed and with the TPQ modeled as alanine. The refinement protocol used for the native structures was followed. The inhibitor molecules were only modeled in the final stages of refinement to ensure that the least biased interpretations of the electron density were made.

Data processing and refinement statistics for all the structures are listed in Table 1.

RESULTS

hDAO Inhibition by Pharmaceutical Compounds. Isoniazid (an antibacterial agent used in the treatment of tuberculosis) (*54*), cimetidine (a potent histamine H_2 receptor antagonist and a type I_1 imidazoline receptor agonist) (*55*), clonidine (an anti-hypertension drug) (*56*, *57*), and two anti-protozoal, aromatic diamidines, pentamidine and berenil (*58*, *59*) were selected for investigation into their inhibitory effects against hDAO.

Isoniazid, pentamidine, and berenil were chosen because of the presence of a primary amine functionality, which could directly react with the TPQ cofactor. Cimetidine and clonidine, on the other hand, do not have this capability. These compounds have structural features that mimic histamine, the preferred substrate for hDAO, and thus have the potential to bind in the active site of this enzyme. While all tested pharmaceutical compounds were inhibitors of hDAO, the effectiveness of individual inhibitors varies from low nanomolar to high micromolar levels (Table 2).

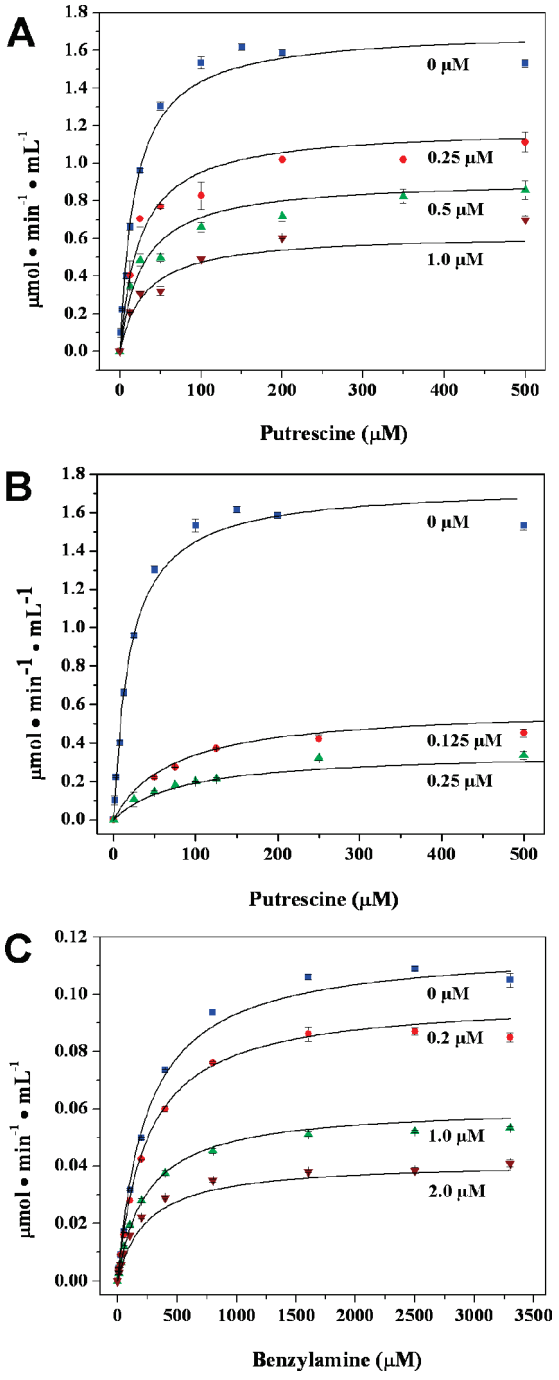

FIGURE 1: Inhibition patterns of hDAO and hVAP. Experimental data curve fits obtained through global model nonlinear regression analysis. (A) Pentamidine inhibition of hDAO [0 (blue squares), 0.25 (red circles), 0.50 (green triangles), and 1.0 μM pentamidine (brown triangles)]. (B). Berenil inhibition of hDAO [0 (blue squares), 0.125 (red circles), and 0.250 μM berenil (green triangles)]. (C). Pentamidine inhibition of hVAP-1 [0 (blue squares), 0.2 (red circles), 1.0 (green triangles), and 2.0 μM pentamidine (brown triangles)].

Nonlinear regression analysis reveals that a mixed type/partial competitive mode of inhibition best describes the nature of inhibition toward putrescine oxidation for hDAO in all but one case (Table 2). Isoniazid is the lone exception, where inhibition is purely noncompetitive with a K_i value of 970 ± 50 μM. The Lineweaver−Burk replot of the nonlinear regression global fits (data not shown) shows these lines converging on the *x*-axis, as expected for noncompetitive inhibition.

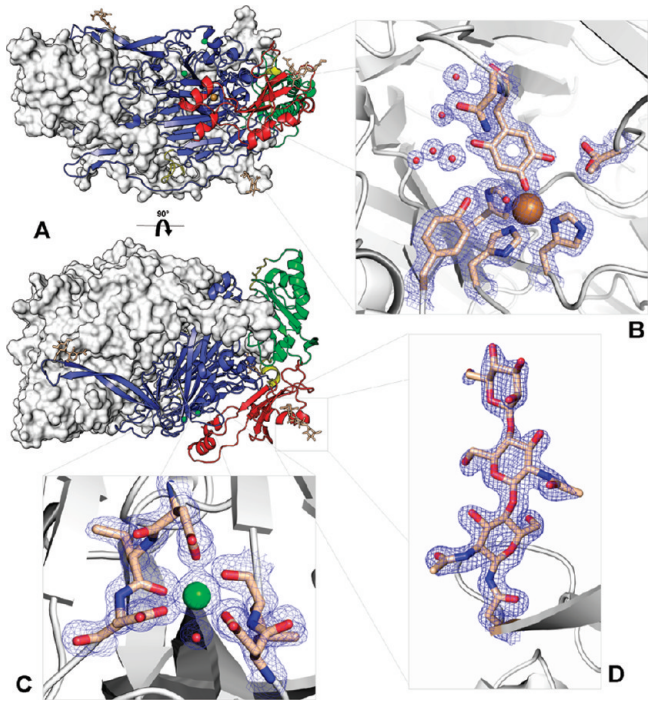

FIGURE 2: (A) View of dimeric hDAO highlighting interesting features. One subunit is shown in a ribbon representation colored by domain (domain 2, red; domain 3, green; domain 4, blue). Linkers joining D2 to D3 and D3 to D4 are colored yellow; Ca^{2+} is colored green, Cu^{2+} brown, and carbohydrate wheat. The second subunit is shown as a molecular surface to highlight the dimeric interaction of the subunits. (B) Active site of one subunit of hDAO. (C) One of the two Ca^{2+} binding sites in each subunit. (D) Glycosylation at Asn110, one of three glycosylation sites per subunit. The $2F_o - F_c$ electron density maps are contoured at 1.5σ.

Pentamidine and berenil, two benzamidine derivatives, are the most potent inhibitors of hDAO, with K_i values in the nanomolar range. Both these compounds exhibit mixed type/partial competitive inhibition toward putrescine oxidation (Figure 1A,B). Double-reciprocal plots of the nonlinear regression global fits show an off-axis intersection point, as expected for this type of inhibition model (data not shown). In contrast, pentamidine inhibition of hVAP is purely noncompetitive with a K_i value of 1.10 ± 0.04 μM (Figure 1C).

Crystal Structures of hDAO. The native structure of hDAO and those of the berenil and pentamidine complexes have been refined at 1.8, 2.1, and 2.2 Å resolution, respectively, with good geometry and low *R* values (Table 1). A structure alignment of 1425 Cα atoms of the native structure with those of berenil and pentamidine yields root-mean-square deviations (rmsd) of 0.11 and 0.13 Å, respectively. Given the precision of these structures (Table 1), we can conclude that the structures are essentially identical and that a general description can be made on the basis of the native structure alone. Important differences between the native and inhibitor structures will be discussed separately.

hDAO is a homodimer of two 85 kDa subunits (A and B) (Figure 2A). There is one homodimer present in the asymmetric unit, formed from residues A27−A267 and A278−A751 from one subunit and residues B28−B263 and B278−B751 from the other. There is only very weak electron density for one additional residue at the N-terminus of chain B. The missing residues at the N-terminus include the 19-residue signal peptide that was omitted from the construct. Therefore, residues 20−26 in the A chain and 20−27 in the B chain are likely to be disordered.

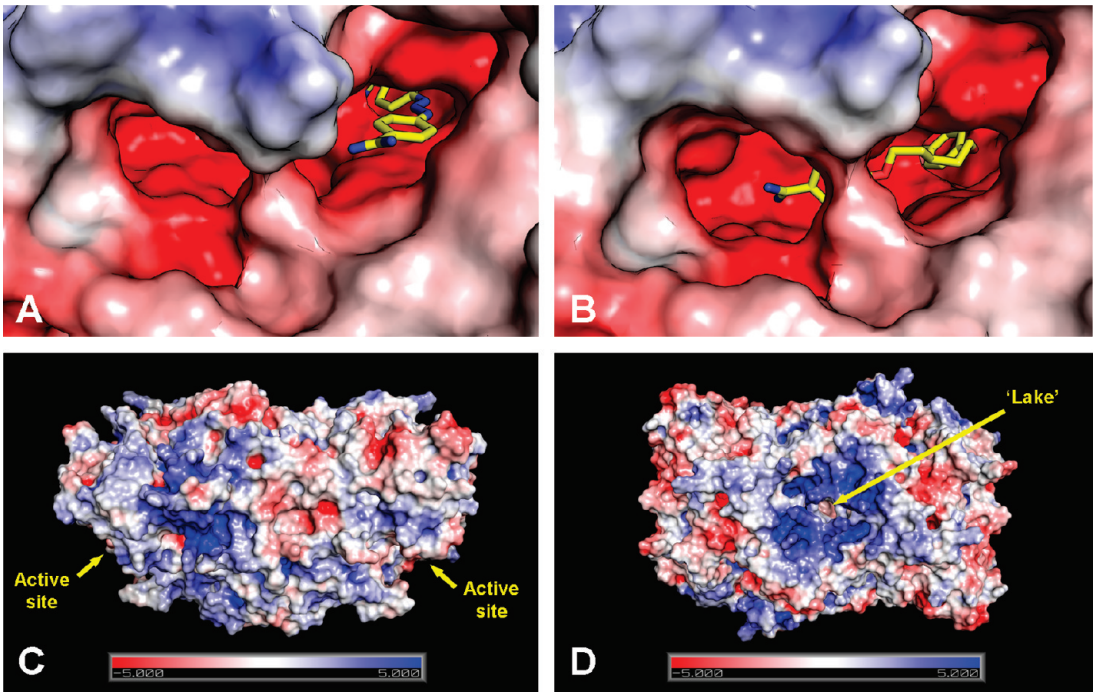

FIGURE 3: Solvent accessible molecular surface representations of the hDAO dimer colored by electrostatic potential (kT/e) at concentrations of 0.15 M for −1 and +1 ionic species at pH 7.0. (A and B) Zoomed-in views of berenil and pentamidine, respectively, bound in the hDAO active-site cavity. The TPQ is hidden from view beneath the right-hand side of each inhibitor shown as a stick representation (yellow). (C) Lateral view of the hDAO dimer. (D) Top view of the hDAO dimer.

Similarly, there is only weak uninterpretable electron density for loops from residues 268−277 in the A chain and from residues 264−277 in the B chain. No residues are missing from the C-terminus of the mature protein.

Structurally, hDAO is very similar to the other reported CAO structures (*27*). It shares the archetypal CAO fold comprised of the three domains, D2, D3, and D4, from each subunit that make up the mushroom cap (Figure 2A). The D1 domain is a unique feature of the *E. coli* enzyme among those that have been structurally characterized. The dimer interface is formed by residues from the D4 units that form an annulus at the center and extensive areas of contact made by arms that reach across from one subunit to the other. The total buried surface is 8597 Å^2 per monomer, of which the arms account for 4079 Å^2 (*60*). The D2 and D3 domains lie at the periphery of the cap (Figure 2A). Domain 2 consists of residues 27−135. Connecting D2 to D3 is a short linker of eight residues. Domain 3 extends from residue 144 to 258. Both D2 and D3 are similar in length and are composed of a four-stranded β-sheet and three α-helices. It has been proposed that the D2 and D3 domains arose from an early gene duplication event (*28*). They have no specific known function other than a structural role. Bridging from one side of the structure to the other, and linking D3 to D4, is a meandering 51-residue linker that threads beneath the center of the two D4 domains before joining to the larger of the two central β-sheets that start domain D4. This linker contains the disordered loop corresponding to residues 267−278. The largest domain, D4, is comprised of residues 310−751 and contains the active site and the protruding arms linking the subunits. Arm 1, termed the "upper arm" (*30*), consists of residues 529−559 and is an extended β-hairpin. The "lower arm" consists of a four-stranded β-sheet comprised of residues from two sections of the polypeptide chain (427−446 and 712−730). Each of the D4 subunits is dominated by a central β-sandwich comprising twisted eight- and six-stranded β-sheets. The active site of each subunit is located between and toward the edge of these β-sheets with both contributing elements of the active site.

Copper Binding Site. The active site of hDAO (Figure 2B) contains a type II copper ion coordinated in a distorted tetrahedral geometry by the $N^{\epsilon 2}$ atoms of the imidazole side chains of His510 and His512 and the $N^{\delta 1}$ atom of His675 and the O4 atom of the TPQ cofactor. In all the structures described here, the TPQ is in the on-copper conformation. The TPQ was actually modeled as a 50:50 mixture of TPQ and tyrosine on the basis of earlier experiments that showed approximately 1 mol of TPQ per dimer was formed in the insect cell expression system (*18*). Consistent with the description of the partial formation of TPQ, Thr685 is also present in two conformations, each with an occupancy of 0.5, one of which forms a hydrogen bond with the O5 atom of TPQ.

Other Metal Binding Sites. In addition to the copper ion in the active site, there are two other cation binding sites per subunit. These have been modeled as Ca^{2+} ions. The first calcium (Figure 2C) is present in all CAO structures except for HPAO and has therefore been suggested to play an as yet unknown functional or structural role (*27*). This calcium has an octahedral geometry with oxygen ligands from one water molecule, the carboxylate groups of three aspartic acid residues (Asp519, Asp521, and Asp664), and the carbonyl oxygen atoms of Leu520 and Leu665. These ligands are completely conserved in the bovine serum and hVAP-1 structures. The second Ca^{2+} is coordinated by seven oxygen atoms from two water molecules, the carboxylate group of Glu562 acting as a bidentate ligand, the side chains of Asn656 and Glu658, and the carbonyl oxygen of Phe653. The ligands for this second Ca^{2+} site are also conserved in the other mammalian enzymes, hVAP-1 and BSAO. A Ca^{2+} ion is also present in PPLO and ECAO close to this site but with different ligand residues.

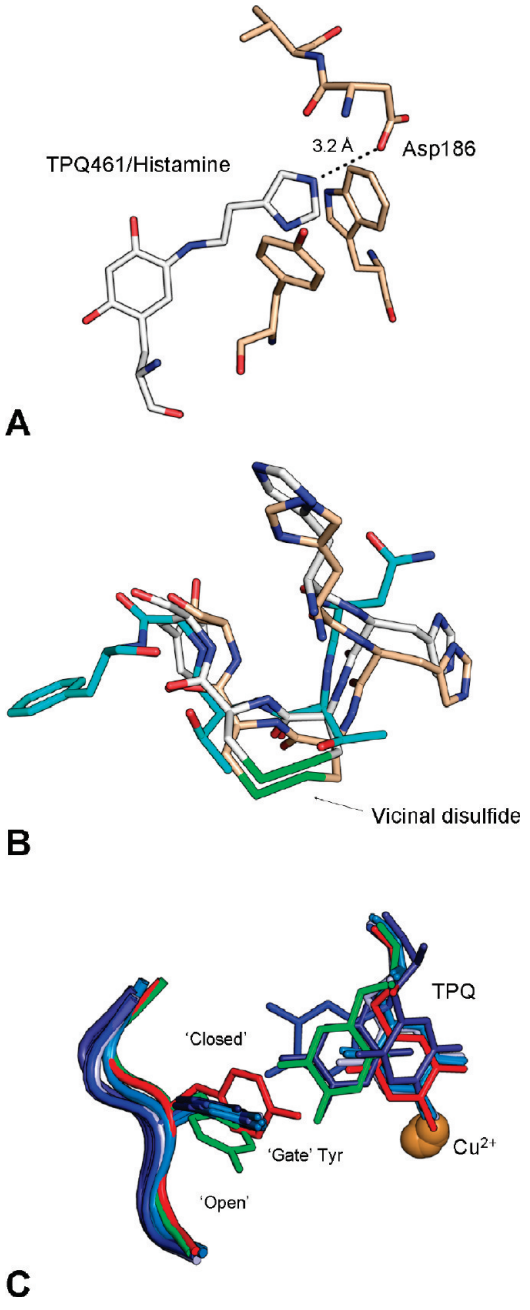

FIGURE 4: (A) Model of histamine, off-copper TPQ Schiff base intermediate as it would appear during catalysis. The imidazole nitrogen of histamine is shown to be well-placed to make a proposed H-bond to Asp186. (B) Native hDAO (cyan) in the region of the vicinal disulfide (green) observed in VAP-1 (white, 2c10) and BSAO wheat, 2pnc). (C) Position of the tyrosine gate in AGAO in the open (green, 2cg0) and closed (red, 1avl) positions with an overlay of all reported mammalian CAO structures (BSAO, 1tu5, 2pnc; VAP-1, 2c10, 2c11, 1us1; hDAO, 3hi7, 3hig, 3hii) shown in shades of blue.

Substrate Channel. The amine substrates of CAOs need to reach the TPQ cofactors in the active site. The active sites of CAOs are quite buried and can be reached only from the enzyme surface by access down a channel that varies in shape and depth depending on the source of the enzyme (*30*). The channel in ECAO is very long and narrow; in marked contrast, the channel in PPLO is a wide open funnel. In hDAO, the active-site channel appears from the surface as a narrow asymmetrical cone-shaped cavity that divides into two and later recombines near the TPQ cofactor (Figure 3A,B). The cavity dimensions are approximately 26 Å × 13 Å × 9 Å. An electrostatic rendering of the surface of hDAO (Figure 3A,B) shows that the lining of the channel is negatively charged as might be expected for an enzyme that acts on positively charged amine substrates. In the structures of ECAO, AGAO, and PSAO, a tyrosine residue acts as a gate across the lower part of the channel blocking access to the TPQ when closed. The structurally equivalent residue in hDAO, Tyr371, appears to be halfway between the "open" and "closed" conformations observed in other CAOs and does not appear to block the TPQ from reaching the off-copper conformation or to block access to the TPQ by substrates.

The characteristic feature of hDAO is the presence of an aspartic acid residue, Asp186, halfway down the substrate channel. It is positioned to interact with the second amine group of a diamine substrate such as histamine. A model of histamine in the active site with the TPQ placed in the off-copper conformation is shown in Figure 4A.

The Lake. Analysis of the structure of AGAO first showed the presence of a lake at the dimer interface between the subunits (*61*). Lakes of various sizes were subsequently described in the structures of all CAOs. It has been suggested that the small substrates, O_2, and/or small products, H_2O_2 and NH_3, could enter or leave via this route and therefore avoid conflict with the amine substrate and aldehyde product in the substrate channel (*30*, *61*). The entry to the lake in hDAO is centrally located in the middle of the top of the structure (Figure 3D) with the lake occupying the space between the two subunits. Interestingly, the site of entry into the lake in hDAO is flanked on both sides by a region of positively charged residues (Figure 3D) from either monomer which has previously been recognized as a heparin binding-site consensus sequence (residues 568−575) (*18*).

Glycosylation Sites. Ultracentrifugation of recombinant hDAO expressed in insect cells indicated that the protein contained between 20 and 26% glycosylation by weight (*18*). Oligosaccharide chains have been modeled into good electron density at three of the four putative N-linked sites at Asn110, Asn538, and Asn745. These three asparagines are conserved in all known mammalian diamine oxidases. At least two *N*-acetylglucosamine residues have been modeled at each site. Interestingly, at the Asn110 site in the A subunit, there was sufficient density to allow the modeling of a third mannose residue that was apparently ordered due to contacts made with a symmetry-related molecule in the crystal (Figure 2D). There is no electron density at the fourth potential site, Asn168, suggesting that it is not glycosylated. This site is located on the surface and would provide unhindered access for the glycosyltransferases. However, this asparagine is not conserved in other mammalian diamine oxidases.

Cysteine Residues and Disulfides. Dimeric hDAO contains five disulfide bridges. A conserved intramolecular disulfide observed in all CAO structures except ECAO is present between Cys391 and Cys417. A disulfide between Cys177 and Cys181 stabilizes a short loop. A vicinal disulfide, observed in both BSAO and hVAP-1, is absent in hDAO. Jackobsson and colleagues (*44*) speculated that this vicinal bridge in hVAP-1 could function as a redox switch. It would be formed at a relatively low pH by oxidation with hydrogen peroxide and could possibly induce a conformation change on the surface of the enzyme when reduced. Since hydrogen peroxide is a product of the amine oxidation and that catalase is known to inhibit the effect of SSAO activity on glucose uptake in adipocytes, hydrogen peroxide had been suggested to play a role in this mechanism (*62*). The structures of hDAO, hVAP-1, and BSAO in this

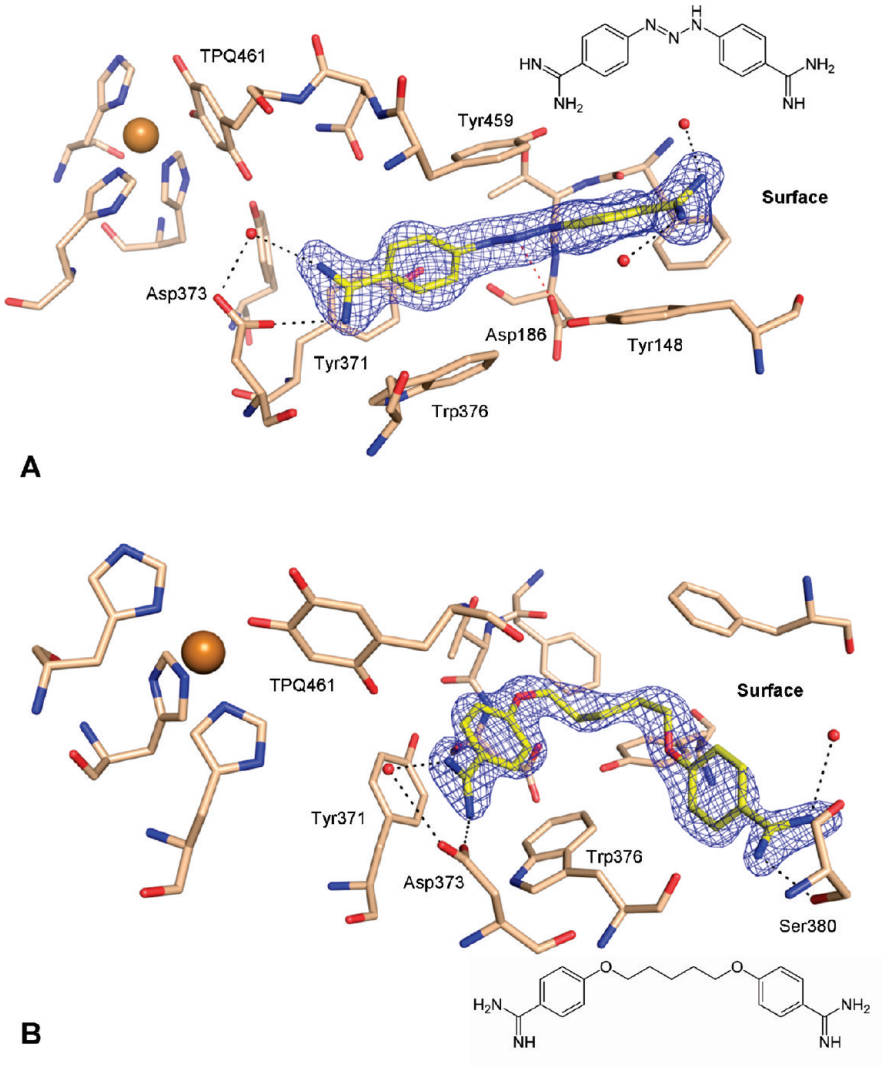

FIGURE 5: (A) Orientation of the molecule berenil (yellow) in the hDAO active-site channel. Hydrogen bonds are shown as black dashed lines. The observed electrostatic interaction between the carboxylate group of Asp186 and the triazene group of berenil is colored red. The molecular structure of berenil is shown in the top right corner. (B) Orientation of the molecule pentamidine within the active site of hDAO. Observed hydrogen bonding is shown with black dashed lines. The molecular structure of pentamidine is shown in the bottom right corner. The $2F_o - F_c$ electron density maps are contoured at 1.3σ.

region (Figure 4B) are very similar despite the lack of the vicinal disulfide in hDAO. This structural similarity casts some doubt on the proposed functional significance of the vicinal disulfide in hVAP-1.

An intermolecular disulfide between Cys736 in the A and B subunits links the dimer. A similar C-terminal intermolecular disulfide has also been observed in PSAO and in one of the two available native hVAP-1 structures (*63*). In the hVAP-1 structure of Jackobsson and colleagues (*44*), a disulfide between a Cys41 near the N-terminus and Cys748 near the C-terminus was modeled. It was recognized by the authors that this may have been an artifact of their protein preparation as it differed from the model of Airenne et al., in which the disulfide occurs between the Cys748 residues of the two subunits. Our observation in hDAO supports the findings of the hVAP-1 model with the intermolecular disulfide (*63*).

Structure of the Berenil Complex. Omit $F_o - F_c$ density for BRN is very good (Figure S1 of the Supporting Information) and has allowed the inhibitor to be modeled at full occupancy in both active sites of the structure. BRN is in an extended conformation and is noncovalently bonded to the protein, making a number of hydrogen bonds and hydrophobic interactions (Figure 5A). The amidinium group at the end of BRN, more deeply inserted into the active site, makes hydrogen bonds with the two carboxylate oxygen atoms of the putative catalytic base, Asp373. One of these is an indirect hydrogen bond via a water molecule (Figure 5A). The first phenyl ring of BRN forms an offset T-shaped π-stacking interaction with Trp376 and a parallel displaced π-stacking interaction with Tyr371. Parallel displaced π-stacking occurs between the other phenyl ring of BRN and the phenyl ring of Tyr148. The triazene group of BRN makes an electrostatic interaction with Asp186. The three N atoms of the triazine moiety are 2.8, 3.0, and 3.2 Å, respectively, from the closest carboxylate oxygen atom of Asp186. The potential donor and acceptor groups are not oriented suitably for the formation of a hydrogen bond. BRN also makes a number of contacts with four ordered water molecules. BRN displaces at least eight water molecules and a glycerol molecule located in the substrate channel of the native structure. Apart from displacing solvent, BRN introduces very few changes to the residues lining the active-site channel apart from a slight displacement of the indole group of Trp376 probably due to the π-stacking mentioned

above. BRN does not contact the TPQ directly. The closest point of contact is 4.5 Å. The TPQ is well-ordered in its on-copper conformation. The structure indicates that binding of BRN in the active-site channel is incompatible with the off-copper conformation of TPQ.

Structure of the Pentamidine Complex. PNT has been modeled at an occupancy of 0.75 in a similar orientation in both active sites. The reduced occupancy gives similar displacement parameters for the PNT and surrounding residues. In a fashion similar to that of BRN, PNT binds hDAO noncovalently. It adopts a horseshoe conformation (Figure 5B) unlike BRN, which is essentially straight. The more buried amidinium group forms the same hydrogen bonds to Asp373 as observed in the BRN complex, and the first phenyl ring forms the same stacking interactions with Trp376 and Tyr371. The linker region makes no specific contacts with the protein and is weakly resolved in the electron density. Unlike BRN, it does not contact Asp186. The amidinium group that extends out of the active site makes a hydrogen bond to Ser380 which, unlike both the native and BRN complex structures, is well-ordered in one conformation. PNT makes two additional contacts with water molecules and directly displaces a glycerol and eight water molecules observed in the active-site channel of the native structure. At its closest point, PNT lies ~3.9 Å from the TPQ. The TPQ is modeled in an on-copper conformation. There is, however, some residual difference electron density calculated from the final model of the PNT complex that suggests a small proportion of the TPQ may be in its off-copper conformation. This would be consistent with the less than full occupancy of the PNT, which when bound is not compatible with the off-copper conformation of the TPQ.

DISCUSSION

Substrate Specificity. We now have available two human CAO structures, hVAP-1 and from this work hDAO. In any consideration of either as an inhibitor or drug target, it is useful to highlight the structural differences between them and to explore whether these differences can be related to their functions. Despite having a moderate level of sequence identity (~37.9%), the structures of hVAP-1 and hDAO have a rmsd of 1.2 Å for 664 Cα atoms when the proteins are superimposed using the secondary structure matching (SSM) method (*64*). As a consequence, the distribution of secondary structural elements is also highly conserved (Figure S2 of the Supporting Information). However, despite the overall similarity, there are a number of subtle differences in side chain orientation within the active-site channel and a conformation change of one loop at the entrance.

The entrance to the active site is considerably narrower in hDAO than in hVAP-1, resulting from a changed conformation in a loop that defines one boundary of the active-site cavity "lip". This loop is formed from the tip of the top β-hairpin of the lower arm from the other subunit of the dimer involving residues 446−450 in hVAP-1 and 434−440 in hDAO. In hDAO, the longer loop forms a "bridge" between the two sides of the entrance cavity, effectively dividing the opening into two (Figure 3A,B). The active-site entrance of hDAO is further restricted at one end by the C-terminal residues, 747−751.

Other differences that may affect substrate preferences include Tyr152 in hDAO that lies on the lip of the active-site cavity in the position equivalent to that of the negatively charged Asp180 in hVAP-1. Tyr152 is apparently quite mobile since it is observed in two conformations. In hDAO, Ser380 is located in a position to interact with the second amine of longer diamine substrates (see below). The equivalent residue in hVAP-1 is a lysine (Lys393) that would effectively discriminate against longer diamines. All the residues deep in the active site are conserved between hDAO and hVAP-1, with the exception of His486 (hDAO) that is Ser496 in hVAP-1.

The proximity of glycans to the active-site channel attached to Asn232 and Asn294 in hVAP-1 has been suggested to control both enzymatic activity and cell adhesion (*63*). The corresponding residues in hDAO are not asparagine and are therefore not glycosylated. The closest glycan to the active-site cavity of hDAO is attached to Asn745 lying ~25 Å away and would therefore not be in a position to influence entry of the substrate into the active site. In hVAP-1, glycosylation at Asn592, Asn618, and Asn666 has been implicated in cell adhesion (*65*, *66*) and at Asn618 and Asn666 in screening the passage of smaller substrates and products through a secondary passage to the active site (*63*). hDAO is not glycosylated at sites corresponding to these positions. hDAO does share one glycosylation site (Asn110) with a putative site in hVAP-1 (Asn137). However, the role of this glycan in hVAP-1 is unknown (*63*). Functional roles for glycosylation in hDAO have yet to be proposed.

The structure of native hDAO and of its complexes with BRN and PNT can provide a structural explanation for the substrate preference of hDAO. Three residues in particular form specific interactions with BRN and PNT. Asp373 interacts with the more deeply buried amidinium groups of BRN and PNT. However, Asp373 is the catalytic base conserved in all CAOs and cannot therefore be responsible for substrate specificity. Both molecules also make a specific contact via nitrogen groups to key residues within the hDAO active-site cavity. The triazene group of BRN interacts with Asp186 which lies halfway along the active-site cavity wall from the TPQ to the surface. The orientations of the groups indicate that this is an electrostatic interaction and not a hydrogen bond. An alignment of all known diamine oxidase sequences with all copper amine oxidase sequences shows this residue is aspartate in all DAOs but never in other CAOs. For example, when the crystal structures are superposed, it is Thr212 in hVAP-1, Asn211 in BSAO, and Ser214 in PPLO. PNT lacks a positively charged group in the central linker region and is therefore unable to make the equivalent contact with Asp186. This may explain why PNT binds less strongly than BRN. PNT is much longer than BRN and binds in a horseshoe conformation unlike BRN that is essentially straight. Because of its length, PNT is able to make a hydrogen bond to Ser380 that is conserved in all DAOs so far characterized and is absent from all other CAOs. It is tempting to speculate that PNT binds in a similar fashion to diamine substrates similar in length such as spermidine and spermine that also contain long linker regions with amines at either end. However, these substrates also contain a nitrogen group in the linker region able to interact with Asp186 in addition to terminal amines that are available for hydrogen bonding with Ser380. Longer aliphatic diamines such as 1,7-diaminoheptane, 1,8-diaminooctane, and 1,9-diaminononane have also been shown to be lower-affinity substrates of diamine oxidase purified from human intestinal tissue (*24*). Such long extended substrates would be able to interact with Ser180 but lack a positive group in the linker region able to interact with Asp186. One of the best substrates of recombinant hDAO has previously been shown to be histamine (*18*). We have modeled histamine into the active site of hDAO as the substrate Schiff base complex with TPQ in the off-copper conformation (Figure 4A). This places the imidazole

ring in a position to interact with Asp186, providing an explanation for the higher reported affinity for histamine versus those of other diamines (*18*). Putrescine is also an excellent substrate of DAO and similar in length to histamine and could theoretically form a similar interaction with Asp186.

Two structures are currently available showing the binding of inhibitors to the other mammalian CAOs, BSAO and hVAP-1. Despite poor electron density because of a number of experimental difficulties, 2-hydrazinopyridine (2HP) was seen to bind hVAP-1 as a nonhydrolyzable substrate forming a Schiff base complex with the TPQ (*44*). 2HP belongs to a class of irreversible covalently bound substratelike CAO inhibitors which have been well-characterized structurally (*31*, *32*, *67*). There is one structure of a noncovalently bound inhibitor of a mammalian CAO. Clonidine binds to BSAO in a solvent accessible pocket near the active site that forces the TPQ away from its active off-copper conformation and into its on-copper conformation (*35*). We have shown that clonidine is a weak inhibitor of hDAO. In the BSAO complex, clonidine appears to be trapped in an aromatic side chain π-stacking "sandwichlike" interaction with the TPQ and a Tyr residue. The superposition of hDAO and BSAO shows that these residues are conserved and are in similar positions, suggesting clonidine might bind similarly in the two enzymes. The location of clonidine deep within the active site would not prevent substrate from entering the channel. PNT and BRN on the other hand occupy the substrate channel and would prevent the entry of substrate (Figure 3A,D). Interestingly, in all four mammalian CAO inhibitor structures, nitrogen atoms of the inhibitors are involved in hydrogen bonds to the Asp that is the general catalytic base hinting at the importance of preventing the substrate from accessing not only the TPQ but also the Asp. Indeed, it has been suggested previously that the catalytic base accepts a proton from an amine substrate that carries a positive charge when it enters the substrate channel (*68*).

In hVAP-1, Leu469 has been proposed to act as a guardian residue blocking access to the active site (*44*, *63*). The structurally equivalent residue in hDAO is Tyr459 and in all of our structures is positioned to allow unhindered access to the TPQ. However, it is conceivable that it could adopt a conformation that would hinder access to the active site. The structures of hDAO all contain something located in the active-site channel: glycerol in the native structure and either BRN or PNT in the complexes. The presence of these molecules in the active-site channel could be holding Tyr459 in an open conformation.

The work on ECAO, AGAO, HPAO, and PSAO identified residues in the active-site channel that formed a gate blocking access to the TPQ (*27*). In structures of AGAO covalently bound with various inhibitors (*31*, *33*) or in the presence of noncovalently bound molecular wires (*29*, *34*), the gate tyrosine is open, allowing access by substrates and inhibitors, and the TPQ is in its off-copper conformation. This has led to the hypothesis that, in AGAO and possibly other CAOs, substrate (or inhibitor) binding in the active-site channel triggers the opening of the gate that in turn allows the TPQ to adopt its active conformation. hDAO does not appear to follow that paradigm. In all three hDAO structures and in the structures of hVAP-1 and BSAO, the corresponding tyrosine resides in neither an open nor a closed position. The tyrosine side chain appears at the halfway point between the open and closed positions observed in AGAO regardless of the presence of inhibitors and of the TPQ conformation (Figure 4C). This provides evidence that the proposed gate mechanism is not relevant to mammalian CAOs. Further, and at least for hDAO and BSAO, there is no linkage between the presence of an off-copper TPQ and the binding of a molecule in the active-site cavity like there is for AGAO (*29*).

Analyses of inhibitors binding to enzymes that exhibit a ping-pong type reaction mechanism are not always easily explained by traditional inhibition models. There are several different scenarios that may lead to the mixed type inhibition result (Table 2). The most plausible explanation relates to the idea that TPQ exists in an equilibrium between on- and off-copper states in the resting enzyme. Structures of various amine oxidases, in the presence and absence of substrates and substrate analogues, have shown that the mature TPQ cofactor is quite flexible and can readily adopt these conformations (*29*, *31*, *32*). The mixed type inhibition observed with berenil and pentamidine is indicative of an inhibitor binding to various enzyme forms. The structures clearly show that there is a single inhibitor noncovalently bound per active site. It is likely that this noncovalent inhibitor binding may tip the equilibrium toward TPQ adopting a nonproductive conformation (on-copper). In the solution inhibition studies, this would effectively result in a smaller pool of productive TPQ which would be available for oxidation of putrescine, consequently decreasing the apparent V_{max} and increasing the apparent affinity of the substrate for the enzyme, both artifacts of mixed type inhibition profiles.

This work has important physiological relevance in terms of hDAO inhibition by PNT and BRN. Pentamidine, an aromatic diamidine, is an anti-protozoal agent effective against *Pneumocystis carinii* and clinically used in the treatment of *P. carinni* pneumonia (PCP) (*58*, *69*). PCP is an overly common and very serious complication in persons with compromised immune systems, such as cancer patients, transplant recipients, and AIDS patients (*59*, *70*, *71*). Adverse side effects accompanying pentamidine treatment occur in at least 70% of AIDS patients and may include nausea, fever, hypotension, acute renal failure, leukopenia, hypoglycemia, acute pancreatitis, and cardiac arrhythmias (*72*−*78*).

Plasma concentrations of pentamidine isethionate in patients following intravenous treatment have been measured at levels ranging from 25 ng/mL to 1.4 μg/mL (43 nM to 2.3 μM) (*59*, *73*, *79*−*81*). Data also indicate that drug accumulation occurs with multiple dosing events. It is clear that this concentration range would certainly inhibit both hDAO and hVAP-1 activity significantly, perhaps to the point of complete inactivation. The relatively narrow substrate specificity of hVAP-1 indicates that this enzyme has a highly specific function, and in the presence of pentamidine, it may simply lose the ability to transiently bind leukocytes. In contrast, hDAO has broad substrate specificity and can oxidize several physiological amines, including histamine, 1-methylhistamine, putrescine, agmatine, cadaverine, and spermidine (*18*). Therefore, complete inactivation of circulating hDAO or hDAO in tissues by pentamidine could be expected to severely disrupt normal metabolic pathways involving this enzyme. Potentially even more damaging is the fact that the tissue distribution of pentamidine shows that this pharmaceutical accumulates in kidney tissue (*73*, *82*, *83*), a major locus of diamine oxidase expression.

With regard to the potential in vivo effects of diamine oxidase inhibition, circulating histamine concentrations are typically a few micromolar, and we have previously suggested that hDAO likely plays a fundamental role in the metabolism of this amine (*18*). A reasonable hypothesis is that during the course of pentamidine administration (typically 14−21 days) diamine

oxidase activity is essentially eradicated and histamine methyltransferase is unable to sufficiently compensate to clear circulating histamine. This raises the possibility that abnormally high levels of circulating histamine contribute to some of the serious side effects that accompany pentamidine treatment. The correlation between the involvement of histamine in smooth muscle contraction, vasodilation, allergic response, and stimulation of adenylate cyclase activity in neurons (*84*) and certain side effects of pentamidine treatment suggests this may be the case.

Berenil is chemically classified as a diamidine and, along with pentamidine, belongs to the group of benzylamidine derivatives. Berenil is an effective anti-protozoal agent and is used to treat *Trypanosoma* infections. This compound has been used rather sparingly in the treatment of African trypanosomiasis (*85*). It is, however, a more commonly used trypanocide in the treatment of dogs, sheep, horses, and cattle (*86*). In animals, berenil poisoning causes hyperaesthesia, salivation, convulsions, frequent urination and defecation, itching, and sweating, concurrent with liver and kidney damage (*87*).

Berenil has been investigated as a potential inhibitor of polyamine synthesis and degradation through its actions on diamine oxidase, the first step in putrescine degradation, and *S*-adenosylmethionine decarboxylase, which prevents biosynthesis of spermidine and spermine from putrescine (*88*). Administration of berenil to animals suffering from Surra (caused by *Trypanosoma evansi*) caused several allergic reactions, with severity increasing upon subsequent dosages (*89*). It appears as though diamine oxidase was completely inhibited in these animals, thus causing increased circulating histamine levels and the observed allergic response. Supporting evidence for this comes from observations that antihistamines successfully treated the allergic reactions (*89*).

CONCLUSION

The expression, purification, and structural determination of recombinant human diamine oxidase represent a major advance in the study of this human amine oxidase and for the field of CAO research. The substrate specificity of this enzyme (*18*) strongly suggests that human diamine oxidase acts in vivo as a component of multiple metabolic pathways and processes, such as cell proliferation, inflammation, allergic response, and ischemia. Our hypothesis is that some pharmaceuticals may disrupt the normal functions of hDAO in the metabolism of biogenic amines and thus may contribute to deleterious side effects. Particularly noteworthy are the data for the two diamidines, pentamidine and berenil, which are very potent inhibitors of hDAO. It is possible that disruption of normal hDAO amine metabolism may contribute to the side effects and toxicity associated with diamidine treatment. The structural basis of this high-affinity inhibition of hDAO by berenil and pentamidine reveals that this inhibition is noncovalent. This finding should aid the rational design of highly specific hDAO inhibitors and may provide a route to drug design using reversible (noncovalent) inhibitors. Moreover, these structures provide the means to ensure that inhibitors of hVAP-1 do not also inhibit hDAO. This is a plausible goal as the development of selective inhibitors has already been demonstrated for copper amine oxidases given variations in substrate analogue structure coupled with differences in active-site channel architecture (*33*, *34*, *90*). This is increasingly important for the human copper amine oxidase enzymes as hVAP-1 inhibitors are being developed to treat a number of conditions (*91*−*93*).

ACKNOWLEDGMENT

Some of the data for this research were recorded on the 3BM1 beamline at the Australian Synchrotron (Victoria, Australia).

SUPPORTING INFORMATION AVAILABLE

Omit $F_o - F_c$ difference electron density for BRN (Figure S1) and a sequence alignment of hDAO with hVAP-1 depicting secondary structural features extracted from the crystal structure models (Figure S2). This material is available free of charge via the Internet at http://pubs.acs.org.

REFERENCES

1. Schwelberger, H. G. (2006) Origins of plasma amine oxidases in different mammalian species. *Inflammation Res. 55* (Suppl. 1), S57–S58.
2. Imamura, Y., Noda, S., Mashima, Y., Kudoh, J., Oguchi, Y., and Shimizu, N. (1998) Human retina-specific amine oxidase: Genomic structure of the gene (AOC2), alternatively spliced variant, and mRNA expression in retina. *Genomics 51*, 293–298.
3. Imamura, Y., Kubota, R., Wang, Y., Asakawa, S., Kudoh, J., Mashima, Y., Oguchi, Y., and Shimizu, N. (1997) Human retina-specific amine oxidase (RAO): cDNA cloning, tissue expression, and chromosomal mapping. *Genomics 40*, 277–283.
4. Kaitaniemi, S., Elovaara, H., Gron, K., Kidron, H., Liukkonen, J., Salminen, T., Salmi, M., Jalkanen, S., and Elima, K. (2009) The unique substrate specificity of human AOC2, a semicarbazide-sensitive amine oxidase. *Cell. Mol. Life Sci. 66*, 2743–2757.
5. Smith, D. J., Salmi, M., Bono, P., Hellman, J., Leu, T., and Jalkanen, S. (1998) Cloning of vascular adhesion protein 1 reveals a novel multifunctional adhesion molecule. *J. Exp. Med. 188*, 17–27.
6. Salmi, M., Yegutkin, G. G., Lehvonen, R., Koskinen, K., Salminen, T., and Jalkanen, S. (2001) A cell surface amine oxidase directly controls lymphocyte migration. *Immunity 14*, 265–276.
7. Salmi, M., and Jalkanen, S. (2001) VAP-1: An adhesin and an enzyme. *Trends Immunol. 22*, 211–216.
8. Koskinen, K., Vainio, P. J., Smith, D. J., Pihlavisto, M., Yla-Herttuala, S., Jalkanen, S., and Salmi, M. (2004) Granulocyte transmigration through the endothelium is regulated by the oxidase activity of vascular adhesion protein-1 (VAP-1). *Blood 103*, 3388–3395.
9. O′Sullivan, J., Unzeta, M., Healy, J., O'Sullivan, M. I., Davey, G., and Tipton, K. F. (2004) Semicarbazide-sensitive amine oxidases: Enzymes with quite a lot to do. *Neurotoxicology 25*, 303–315.
10. Kurkijarvi, R., Adams, D. H., Leino, R., Mottonen, T., Jalkanen, S., and Salmi, M. (1998) Circulating form of human vascular adhesion protein-1 (VAP-1): Increased serum levels in inflammatory liver diseases. *J. Immunol. 161*, 1549–1557.
11. Gokturk, C., Garpenstrand, H., Nilsson, J., Nordquist, J., Oreland, L., and Forsberg-Nilsson, K. (2003) Studies on semicarbazide-sensitive amine oxidase in patients with diabetes mellitus and in transgenic mice. *Biochim. Biophys. Acta 1647*, 88–91.
12. Obata, T. (2006) Diabetes and semicarbazide-sensitive amine oxidase (SSAO) activity: A review. *Life Sci. 79*, 417–422.
13. Boomsma, F., van Veldhuisen, D. J., de Kam, P. J., Man in't Veld, A. J., Mosterd, A., Lie, K. I., and Schalekamp, M. A. (1997) Plasma semicarbazide-sensitive amine oxidase is elevated in patients with congestive heart failure. *Cardiovasc. Res. 33*, 387–391.
14. Best, C. H. (1929) The disappearance of histamine from autolysing lung tissue. *J. Physiol. 67*, 256–263.
15. Barbry, P., Champe, M., Chassande, O., Munemitsu, S., Champigny, G., Lingueglia, E., Maes, P., Frelin, C., Tartar, A., and Ullrich, A..; et al. (1990) Human kidney amiloride-binding protein: cDNA structure and functional expression. *Proc. Natl. Acad. Sci. U.S.A. 87*, 7347–7351.
16. Novotny, W. F., Chassande, O., Baker, M., Lazdunski, M., and Barbry, P. (1994) Diamine oxidase is the amiloride-binding protein and is inhibited by amiloride analogues. *J. Biol. Chem. 269*, 9921–9925.
17. Chassande, O., Renard, S., Barbry, P., and Lazdunski, M. (1994) The human gene for diamine oxidase, an amiloride binding protein. Molecular cloning, sequencing, and characterization of the promoter. *J. Biol. Chem. 269*, 14484–14489.
18. Elmore, B. O., Bollinger, J. A., and Dooley, D. M. (2002) Human kidney diamine oxidase: Heterologous expression, purification, and characterization. *J. Biol. Inorg. Chem. 7*, 565–579.

19. Schwelberger, H. G. (2004) Diamine oxidase (DAO) enzyme and gene. In Histamine: Biology and Medical Aspects (Falus, A., Ed.) pp 43−52, SpringMed Publishing, Budapest, Hungary.
20. Maintz, L., and Novak, N. (2007) Histamine and histamine intolerance. *Am. J. Clin. Nutr. 85*, 1185–1196.
21. Maintz, L., Schwarzer, V., Bieber, T., van der Ven, K., and Novak, N. (2008) Effects of histamine and diamine oxidase activities on pregnancy: A critical review. *Hum. Reprod. Update 14*, 485–495.
22. Klocker, J., Matzler, S. A., Huetz, G. N., Drasche, A., Kolbitsch, C., and Schwelberger, H. G. (2005) Expression of histamine degrading enzymes in porcine tissues. *Inflammation Res. 54* (Suppl. 1), S54–S57.
23. Schwelberger, H. G., Hittmair, A., and Kohlwein, S. D. (1998) Analysis of tissue and subcellular localization of mammalian diamine oxidase by confocal laser scanning fluorescence microscopy. *Inflammation Res. 47*, S60–S61.
24. Bieganski, T., Kusche, J., Lorenz, W., Hesterberg, R., Stahlknecht, C. D., and Feussner, K. D. (1983) Distribution and properties of human intestinal diamine oxidase and its relevance for the histamine catabolism. *Biochim. Biophys. Acta 756*, 196–203.
25. Raithel, M., Kufner, M., Ulrich, P., and Hahn, E. G. (1999) The involvement of the histamine degradation pathway by diamine oxidase in manifest gastrointestinal allergies. *Inflammation Res. 48* (Suppl. 1), S75–S76.
26. Schwelberger, H. G. (2007) The origin of mammalian plasma amine oxidases. *J. Neural Transm. 114*, 757–762.
27. Guss, J. M., Zanotti, G., and Salminen, T. (2009) Amine Oxidase Crystal Structures. In Copper Amine Oxidases: Structures, Catalytic Mechanisms and Role in Pathophysiology (Floris, G., and Mondovi, B., Eds.) pp 119−141, Taylor and Francis, Boca Raton, FL.
28. Parsons, M. R., Convery, M. A., Wilmot, C. M., Yadav, K. D., Blakeley, V., Corner, A. S., Phillips, S. E., McPherson, M. J., and Knowles, P. F. (1995) Crystal structure of a quinoenzyme:copper amine oxidase of *Escherichia coli* at 2 Å resolution. *Structure 3*, 1171–1184.
29. Langley, D. B., Brown, D. E., Cheruzel, L. E., Contakes, S. M., Duff, A. P., Hilmer, K. M., Dooley, D. M., Gray, H. B., Guss, J. M., and Freeman, H. C. (2008) Enantiomer-specific binding of ruthenium(II) molecular wires by the amine oxidase of *Arthrobacter globiformis*. *J. Am. Chem. Soc. 130*, 8069–8078.
30. Duff, A. P., Cohen, A. E., Ellis, P. J., Kuchar, J. A., Langley, D. B., Shepard, E. M., Dooley, D. M., Freeman, H. C., and Guss, J. M. (2003) The crystal structure of *Pichia pastoris* lysyl oxidase. *Biochemistry 42*, 15148–15157.
31. Langley, D. B., Trambaiolo, D. M., Duff, A. P., Dooley, D. M., Freeman, H. C., and Guss, J. M. (2008) Complexes of the copper-containing amine oxidase from *Arthrobacter globiformis* with the inhibitors benzylhydrazine and tranylcypromine. *Acta Crystallogr. F64*, 577–583.
32. Wilmot, C. M., Murray, J. M., Alton, G., Parsons, M. R., Convery, M. A., Blakeley, V., Corner, A. S., Palcic, M. M., Knowles, P. F., McPherson, M. J., and Phillips, S. E. (1997) Catalytic mechanism of the quinoenzyme amine oxidase from *Escherichia coli*: Exploring the reductive half-reaction. *Biochemistry 36*, 1608–1620.
33. O'Connell, K. M., Langley, D. B., Shepard, E. M., Duff, A. P., Jeon, H. B., Sun, G., Freeman, H. C., Guss, J. M., Sayre, L. M., and Dooley, D. M. (2004) Differential inhibition of six copper amine oxidases by a family of 4-(aryloxy)-2-butynamines: Evidence for a new mode of inactivation. *Biochemistry 43*, 10965–10978.
34. Contakes, S. M., Juda, G. A., Langley, D. B., Halpern-Manners, N. W., Duff, A. P., Dunn, A. R., Gray, H. B., Dooley, D. M., Guss, J. M., and Freeman, H. C. (2005) Reversible inhibition of copper amine oxidase activity by channel-blocking ruthenium(II) and rhenium(I) molecular wires. *Proc. Natl. Acad. Sci. U.S.A. 102*, 13451–13456.
35. Holt, A., Smith, D. J., Cendron, L., Zanotti, G., Rigo, A., and Di Paolo, M. L. (2008) Multiple binding sites for substrates and modulators of semicarbazide-sensitive amine oxidases: Kinetic consequences. *Mol. Pharmacol. 73*, 525–538.
36. Brown, D. G., Sanderson, M. R., Garman, E., and Neidle, S. (1992) Crystal-Structure of a Berenil-D(Cgcaaatttgcg) Complex: An Example of Drug DNA Recognition Based on Sequence-Dependent Structural Features. *J. Mol. Biol. 226*, 481–490.
37. Edwards, K. J., Jenkins, T. C., and Neidle, S. (1992) Crystal structure of a pentamidine-oligonucleotide complex: Implications for DNA-binding properties. *Biochemistry 31*, 7104–7109.
38. Szutowicz, A., Kobes, R. D., and Orsulak, P. J. (1984) Colorimetric Assay for Monoamine-Oxidase in Tissues Using Peroxidase and 2,2′-Azinodi(3-Ethylbenzthiazoline-6-Sulfonic Acid) as Chromogen. *Anal. Biochem. 138*, 86–94.
39. Holt, A., Degenhardt, O. S., Berry, P. D., Kapty, J. S., Mithani, S., Smith, D. J., and Di Paolo, M. L. (2007) The effects of buffer cations on interactions between mammalian copper-containing amine oxidases and their substrates. *J. Neural Transm. 114*, 733–741.
40. Tabor, C. W., Tabor, H., and Rosenthal, S. M. (1954) Purification of Amine Oxidase from Beef Plasma. *J. Biol. Chem. 208*, 645–661.
41. Juda, G. A., Shepard, E. M., Elmore, B. O., and Dooley, D. M. (2006) A comparative study of the binding and inhibition of four copper-containing amine oxidases by azide: Implications for the role of copper during the oxidative half-reaction. *Biochemistry 45*, 8788–8800.
42. Segel, I. H. (1975) Enzyme kinetics: Behavior and analysis of rapid equilibrium and steady-state systems , John Wiley & Sons, New York.
43. Otwinowski, Z., and Minor, W. (1997) Processing of X-ray diffraction data collected in oscillation mode. *Methods Enzymol. 276*, 307–326.
44. Jakobsson, E., Nilsson, J., Ogg, D., and Kleywegt, G. J. (2005) Structure of human semicarbazide-sensitive amine oxidase/vascular adhesion protein-1. *Acta Crystallogr. D61*, 1550–1562.
45. Stein, N. (2008) CHAINSAW: A program for mutating pdb files used as templates in molecular replacement. *J. Appl. Crystallogr. 41*, 641–643.
46. McCoy, A. J. (2007) Solving structures of protein complexes by molecular replacement with Phaser. *Acta Crystallogr. D63*, 32–41.
47. Murshudov, G. N., Vagin, A. A., and Dodson, E. J. (1997) Refinement of macromolecular structures by the maximum-likelihood method. *Acta Crystallogr. D53*, 240–255.
48. Afonine, P. V., Grosse-Kunstleve, R. W., and Adams, P. D. (2005) The Phenix refinement framework, CCP4 Newsletter , Vol. 42.
49. Emsley, P., and Cowtan, K. (2004) Coot: Model-building tools for molecular graphics. *Acta Crystallogr. D60*, 2126–2132.
50. Leslie, A. G. W. (1992) Recent changes to the MOSFLM package for processing film and image plate data, Joint CCP4 + ESF-EAMCB Newsletter on Protein Crystallography , Vol. 26.
51. Collaborative Computational Project No. 4 (1994) The CCP4 suite: Programs for protein crystallography. *Acta Crystallogr. D50*, 760–763.
52. Davis, I. W., Leaver-Fay, A., Chen, V. B., Block, J. N., Kapral, G. J., Wang, X., Murray, L. W., Arendall, W. B., Snoeyink, J., Richardson, J. S., and Richardson, D. C. (2007) MolProbity: All-atom contacts and structure validation for proteins and nucleic acids. *Nucleic Acids Res. 35*, W375–W383.
53. Cruickshank, D. W. J. (1999) Remarks about protein structure precision. *Acta Crystallogr. D55*, 583–601.
54. Potter, B., Rindfleisch, K., and Kraus, C. K. (2005) Management of active tuberculosis. *Am. Fam. Physician 72*, 2225–2232.
55. van der Goot, H., and Timmerman, H. (2000) Selective ligands as tools to study histamine receptors. *Eur. J. Med. Chem. 35*, 5–20.
56. Head, G. A., Chan, C. K. S., and Burke, S. L. (1998) Relationship between imidazoline and α(2)-adrenoceptors involved in the sympatho-inhibitory actions of centrally acting antihypertensive agents. *J. Auton. Nerv. Syst. 72*, 163–169.
57. Khan, Z. P., Ferguson, C. N., and Jones, R. M. (1999) α-2 and imidazoline receptor agonists: Their pharmacology and therapeutic role. *Anaesthesia 54*, 146–165.
58. Bray, P. G., Barrett, M. P., Ward, S. A., and de Koning, H. P. (2003) Pentamidine uptake and resistance in pathogenic protozoa: Past, present and future. *Trends Parasitol. 19*, 232–239.
59. Fishman, J. A. (1998) Treatment of infection due to *Pneumocystis carinii*. *Antimicrob. Agents Chemother. 42*, 1309–1314.
60. Krissinel, E., and Henrick, K. (2007) Inference of macromolecular assemblies from crystalline state. *J. Mol. Biol. 372*, 774–797.
61. Wilce, M. C., Dooley, D. M., Freeman, H. C., Guss, J. M., Matsunami, H., McIntire, W. S., Ruggiero, C. E., Tanizawa, K., and Yamaguchi, H. (1997) Crystal structures of the copper-containing amine oxidase from *Arthrobacter globiformis* in the holo and apo forms: Implications for the biogenesis of topaquinone. *Biochemistry 36*, 16116–16133.
62. Zorzano, A., Abella, A., Marti, L., Carpene, C., Palacin, M., and Testar, X. (2003) Semicarbazide-sensitive amine oxidase activity exerts insulin-like effects on glucose metabolism and insulin-signaling pathways in adipose cells. *Biochim. Biophys. Acta 1647*, 3–9.
63. Airenne, T. T., Nymalm, Y., Kidron, H., Smith, D. J., Pihlavisto, M., Salmi, M., Jalkanen, S., Johnson, M. S., and Salminen, T. A. (2005) Crystal structure of the human vascular adhesion protein-1: Unique structural features with functional implications. *Protein Sci. 14*, 1964–1974.
64. Krissinel, E., and Henrick, K. (2004) Secondary-structure matching (SSM), a new tool for fast protein structure alignment in three dimensions. *Acta Crystallogr. D60*, 2256–2268.

65. Salminen, T. A., Smith, D. J., Jalkanen, S., and Johnson, M. S. (1998) Structural model of the catalytic domain of an enzyme with cell adhesion activity: Human vascular adhesion protein-1 (HVAP-1) D4 domain is an amine oxidase. *Protein Eng. 11*, 1195–1204.
66. Maula, S. M., Salminen, T., Kaitaniemi, S., Nymalm, Y., Smith, D. J., and Jalkanen, S. (2005) Carbohydrates located on the top of the "cap" contribute to the adhesive and enzymatic functions of vascular adhesion protein-1. *Eur. J. Immunol. 35*, 2718–2727.
67. Mure, M., Brown, D. E., Saysell, C., Rogers, M. S., Wilmot, C. M., Kurtis, C. R., McPherson, M. J., Phillips, S. E. V., Knowles, P. F., and Dooley, D. M. (2005) Role of the interactions between the active site base and the substrate Schiff base in amine oxidase catalysis. Evidence from structural and spectroscopic studies of the 2-hydrazinopyridine adduct of *Escherichia coli* amine oxidase. *Biochemistry 44*, 1568–1582.
68. Saysell, C. G., Tambyrajah, W. S., Murray, J. M., Wilmot, C. M., Phillips, S. E. V., McPherson, M. J., and Knowles, P. F. (2002) Probing the catalytic mechanism of *Escherichia coli* amine oxidase using mutational variants and a reversible inhibitor as a substrate analogue. *Biochem. J. 365*, 809–816.
69. Goa, K. L., and Campolirichards, D. M. (1987) Pentamidine Isethionate: A Review of Its Antiprotozoal Activity, Pharmacokinetic Properties and Therapeutic Use in *Pneumocystis carinii* Pneumonia. *Drugs 33*, 242–258.
70. Dohn, M. N., Baughman, R. P., Vigdorth, E. M., and Frame, D. L. (1992) Equal survival rates for first, second, and third episodes of *Pneumocystis carinii* pneumonia in patients with acquired immunodeficiency syndrome. *Arch. Intern. Med. 152*, 2465–2470.
71. Goodwin, S. D. (1993) *Pneumocystis carinii* pneumonia in human immunodeficiency virus-infected infants and children. *Pharmacotherapy 13*, 640–646.
72. OBrien, J. G., Dong, B. J., Coleman, R. L., Gee, L., and Balano, K. B. (1997) A 5-year retrospective review of adverse drug reactions and their risk factors in human immunodeficiency virus-infected patients who were receiving intravenous pentamidine therapy for *Pneumocystis carinii* pneumonia. *Clin. Infect. Dis. 24*, 854–859.
73. Sands, M., Kron, M. A., and Brown, R. B. (1985) Pentamidine: A Review. *Rev. Infect. Dis. 7*, 625–634.
74. Balslev, U., and Nielsen, T. L. (1992) Adverse Effects Associated with Intravenous Pentamidine Isethionate as Treatment of *Pneumocystis carinii* Pneumonia in AIDS Patients. *Dan. Med. Bull. 39*, 366–368.
75. Sensakovic, J. W., Suarez, M., Perez, G., Johnson, E. S., and Smith, L. G. (1985) Pentamidine Treatment of *Pneumocystis carinii* Pneumonia in the Acquired Immunodeficiency Syndrome: Association with Acute Renal Failure and Myoglobinuria. *Arch. Intern. Med. 145*, 2247–2247.
76. Briceland, L. L., and Bailie, G. R. (1991) Pentamidine-Associated Nephrotoxicity and Hyperkalemia in Patients with AIDS. *DICP, Ann. Pharmacother. 25*, 1171–1174.
77. Hughes, W. T. (1991) Prevention and Treatment of *Pneumocystis carinii* Pneumonia. *Annu. Rev. Med. 42*, 287–295.
78. Teruya, K., Yasuoka, A., Yamaguchi, M., Yasuoka, C., Yamamoto, Y., Genka, I., Tachikawa, N., Kikuchi, Y., and Oka, S. (2001) Complications during clinical courses of *Pneumocystis carinii* pneumonia in patients with acquired immunodeficiency syndrome. *Intern. Med. 40*, 221–226.
79. Conte, J. E., Chernoff, D., Feigal, D. W., Joseph, P., Mcdonald, C., and Golden, J. A. (1990) Intravenous or Inhaled Pentamidine for Treating *Pneumocystis carinii* Pneumonia in AIDS: A Randomized Trial. *Ann. Intern. Med. 113*, 203–209.
80. Conte, J. E. (1991) Pharmacokinetics of Intravenous Pentamidine in Patients with Normal Renal-Function or Receiving Hemodialysis. *J. Infect. Dis. 163*, 169–175.
81. Conte, J. E.Jr., Upton, R. A., and Lin, E. T. (1987) Pentamidine pharmacokinetics in patients with AIDS with impaired renal function. *J. Infect. Dis. 156*, 885–890.
82. Donnelly, H., Bernard, E. M., Rothkotter, H., Gold, J. W. M., and Armstrong, D. (1988) Distribution of Pentamidine in Patients with AIDS. *J. Infect. Dis. 157*, 985–989.
83. Waalkes, T. P., and Makulu, D. R. (1976) Pharmacologic aspects of pentamidine. *Natl. Cancer Inst. Monogr. 43*, 171–177.
84. Rangachari, P. K. (1992) Histamine: Mercurial Messenger in the Gut. *Am. J. Physiol. 262*, G1–G13.
85. Abaru, D. E., Liwo, D. A., Isakina, D., and Okori, E. E. (1984) Retrospective Long-Term Study of Effects of Berenil by Follow-up of Patients Treated since 1965. *Tropenmed. Parasitol. 35*, 148–150.
86. Peregrine, A. S., and Mamman, M. (1993) Pharmacology of Diminazene: A Review. *Acta Trop. 54*, 185–203.
87. Homeida, A. M., Elamin, E. A., Adam, S. E. I., and Mahmoud, M. M. (1981) Toxicity of Diminazene Aceturate (Berenil) to Camels. *J. Comp. Pathol. 91*, 355–360.
88. Balanafouce, R., Pulido, T. G., Ordonezescudero, D., and Garridopertierra, A. (1986) Inhibition of Diamine Oxidase and S-Adenosylmethionine Decarboxylase by Diminacene Aceturate (Berenil). *Biochem. Pharmacol. 35*, 1597–1600.
89. Tuntasuvan, D., Jarabrum, W., Viseshakul, N., Mohkaew, K., Borisutsuwan, S., Theeraphan, A., and Kongkanjana, N. (2003) Chemotherapy of surra in horses and mules with diminazene aceturate. *Vet. Parasitol. 110*, 227–233.
90. Shepard, E. M., Smith, J., Elmore, B. O., Kuchar, J. A., Sayre, L. M., and Dooley, D. M. (2002) Towards the development of selective amine oxidase inhibitors: Mechanism-based inhibition of six copper containing amine oxidases. *Eur. J. Biochem. 269*, 3645–3658.
91. Stolen, C. M., Marttila-Ichihara, F., Koskinen, K., Yegutkin, G. G., Turja, R., Bono, P., Skurnik, M., Hanninen, A., Jallkanen, S., and Salmi, M. (2005) Absence of the endothelial oxidase AOC3 leads to abnormal leukocyte traffic in vivo. *Immunity 22*, 105–115.
92. Merinen, M., Irjala, H., Salmi, M., Jaakkola, I., Hanninen, A., and Jalkanen, S. (2005) Vascular adhesion protein-1 is involved in both acute and chronic inflammation in the mouse. *Am. J. Pathol. 166*, 793–800.
93. Vainio, P. J., Kortekangas-Savolainen, O., Mikkola, J. H., Jaakkola, K., Kalimo, K., Jalkanen, S., and Veromaa, T. (2005) Safety of blocking vascular adhesion protein-1 in patients with contact dermatitis. *Basic Clin. Pharmacol. Toxicol. 96*, 429–435.